 https://doi.org/10.3311/PPci.19508
Creative Commons Attribution

Periodica Polytechnica Transportation Engineering, 66(4), pp. 1014–1022, 2022

Vibration Assessment of a New Danube Bridge at Komárom

Gergely Szabó[1*], István Völgyi[2], Ágnes Kenéz[2]

[1] Pont-TERV Ltd. Engineering Consultants, Mohai út 38., H-1119 Budapest, Hungary
[2] Department of Structural Engineering, Faculty of Civil Engineering, Budapest University of Technology and Economics, Műegyetem rkp. 3., H-1111 Budapest, Hungary
[*] Corresponding author, e-mail: mr.gergely.szabo@gmail.com

Received: 10 November 2021, Accepted: 30 May 2022, Published online: 28 June 2022

Abstract

In this paper the vortex induced vibration of a cable-stayed bridge with a main span of 252 m was studied at construction stages. Structural FEM and aerodynamic CFD models were made in order to calculate the vibration amplitude of this slender structure. The damping of the pure steel structure and the effect of the tuned mass dampers were measured through on-site vibration tests. Based on the validated structural dynamics model and the simulated aerodynamic parameters, the vortex induced vibration amplitudes were evaluated and compared with the monitoring data gained from accelerometers and wind sensors attached to the stiffening girder during the most critical construction period.

Keywords

cable-stayed bridge, free cantilever construction, vortex induced vibration, monitoring system

1 Introduction

1.1 Motivation

Slender bridge structures are known to be sensitive to wind effects. A number of wind related phenomena are known, among which vortex induced vibration (VIV) can be considered as the most common one that has been observed at a number of bridges in the past decades. Contrary to self-excited vibration such as flutter, VIV may not cause the failure of the bridge, but can lead to unacceptable vibration amplitudes, nevertheless. VIV mostly occur at completed bridges, but can also appear during construction stages, at which the structure has not reached its final stiffness yet, consequently, is exceptionally sensitive to wind loading.

Recently, one of the well-known examples was the intense oscillations of the Volgogradsky Bridge on the 20th May, 2010. The multiple-span continuous girder with maximum spans of 155 m can be considered as extremely flexible due to the low flexural rigidity with natural bending frequencies as low as 0.42 Hz. The vibration modes were almost purely bending. The observed vibration amplitude was estimated as 40 cm. On the 5th May, 2020, the Humen Pearl River Bridge showed remarkable vibration amplitudes. The VIV of the suspension bridge was reportedly caused by the temporary traffic isolation barriers on both sides of the bridge deck installed for maintenance purposes. These elements significantly changed the aerodynamic performance of the otherwise streamlined, closed steel box girder. Although the VIV has not endangered the safety of the structure, the bridge had to be closed. The vibration frequency was 0.368 Hz, corresponding to the third symmetrical vertical bending mode. The estimated amplitude was 31 cm. Although the barriers were removed immediately after the vibrations showed up, the problem has not entirely disappeared. Frequencies of VIV that occurred later were mainly 0.225 Hz and 0.275 Hz, respectively, corresponding to the second symmetrical and the second asymmetrical vertical bending modes. The corresponding amplitudes were 15 cm and 23 cm, respectively [1]. In December of 2020, the Verrazano-Narrows Bridge in New York City was also closed due to high wind velocities and the consequent disturbing vibrations. According to the Metropolitan Transportation Authority, however, the vibration amplitude of the bridge remained on the safe side. VIV mostly occur at completed bridges, but can also appear during construction stages, see e.g., the Alconétar Bridge [2] or the Trans-Tokyo Bay Bridge [3].

1. 2 Problem statement and objectives

Since the vibration amplitudes have to be controlled in order to comply with serviceability (e.g., passenger comfort) and load carrying capacity (fatigue) criteria, the accurate

Cite this article as: Szabó, G., Völgyi, I., Kenéz, Á. "Vibration Assessment of a New Danube Bridge at Komárom", Periodica Polytechnica Civil Engineering, 66(4), pp. 1014–1022, 2022. https://doi.org/10.3311/PPci.19508

calculation of VIV amplitudes is of primary importance. Simplified closed formulas (e.g., Eurocode, [4]), section [5, 6] and full aero-elastic wind tunnel models [7] or fluid-structure interaction simulations [8] are widely used, but there are still uncertainties as to the prediction of the VIV amplitudes [9]. In this paper a slender cable-stayed bridge at Komárom was considered, which was equipped with monitoring sensors during the most critical construction period; therefore, precise wind and vibration data series were available. The main goal was to validate our numerical (structural and fluid dynamics) models in order to improve the reliability of the VIV amplitude calculations.

2 The new Komárom Danube Bridge project

The Komárom Danube Bridge is a cable stayed structure with unusual, one-sided single pylon arrangement, which is therefore fully fixed at the bottom. The main span L is 252 m. The orthotropic deck has trapezoidal ribs and two I-shaped stiffening girders at both sides. The curved cross girders are placed at every 3.00 meters. The deck has a width B of 20.40 m, and a depth D of 2.50 m. The stay cables are composed of A = 150 mm^2 high-grade strands (f_u = 1860 N/mm^2) with a strand number of 43, 55 and 85. The cross section is shown in Fig. 1 with the team of designers ready to make pedestrian excitation tests at the end of the deck. Considering the slenderness of the bridge, 6 pieces of tuned mass dampers (TMD) were installed on the deck in order to mitigate vortex induced vibration. A single TMD has a moving mass, stiffness and damping of M = 5 t, K = 36.5 kN/m and C = 3.4 kNs/m, respectively.

2.1 Construction of the bridge

The bridge was built by using the free cantilever method that is most commonly used for cable stayed bridges. The construction stage-10 can be seen in Fig. 2 with a cantilever length of 209.40 m. Despite the fact, that the TMDs were tuned with respect to the dynamic properties of the completed bridge, the dampers were already erected and activated during the construction stages in order to avoid VIV prior to the deck closure.

2.2 Monitoring system on the bridge

Monitoring system on structures are widely used [10] and was also utilized considering the slenderness of this unique bridge. The dynamic response of the Komárom Bridge as well as the wind velocity were monitored simultaneously by using sensors during the most critical construction period. The sensor positions at the cross section can be seen in Fig. 3. The wind velocity U and direction α were recorded on both sides of the stiffening girder by using sensors type Vaisala WINDCAP Ultrasonic Wind Sensor WXT532 mounted onto high steel masts. The acceleration sensors HBM B12 were installed to the cross sections at the TMD location. The vertical accelerometers were fixed to the top of the moving mass of the TMD (A_{TMD}) as well as to the bridge deck section (A_{bridge}). Thus, the vertical vibration of the bridge deck and the TMD could be measured at the same time. As the length of the stiffening girder changed during the construction, the sensors

Fig. 1 Bridge deck with the designer team (courtesy of Pont-TERV Ltd.)

Fig. 2 Free cantilever of the bridge (courtesy of Pont-TERV Ltd.)

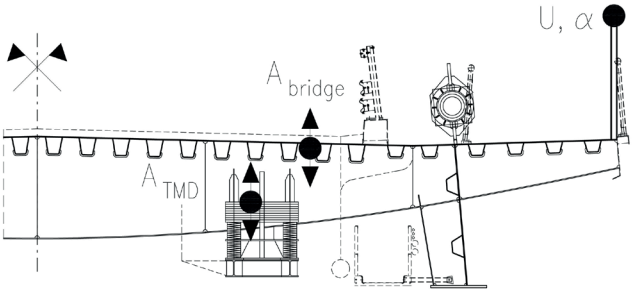

Fig. 3 Sensor positioning at the cross section

were repositioned (at one time only) in order to be closer to the end of the cantilever. Sampling rate for the wind sensors was 1 Hz, while that for the acceleration sensors was 20 Hz. The QuantumX MX840B universal measuring amplifier, the UPS, the PC for the data collection and the GSM communication were placed in a sealed box underneath the deck, near the TMD elements.

3 Structural dynamics of the new Komárom Bridge

In this section the Komárom Bridge is discussed in detail. The FEM model of the bridge (AxisVM software, X4) at stage-10 can be seen in Fig. 4. The orthotropic steel deck with the longitudinal trapezoidal ribs was simplified by using beam elements. The top flanges of the two stiffening girders were defined with respect to the effective width and thickness of the deck plate. The crossbeams at every 3 m were merged into one beam at every 24 m; therefore, the stiffness and mass properties were adjusted adequately. The pylon was also modelled by using beams. The stay cables were modelled by using truss elements. The second order effect of the cable tension forces on the dynamic properties was included. The vibration amplitudes to be determined were expected to be moderate; therefore, modal analysis was utilized, which is based on linearity.

In Fig. 4 the first bending mode shape is also illustrated over the FEM model. The corresponding natural frequency is $f = 0.363$ Hz. At the next stage, a new deck segment was erected and welded, and a new cable pair was installed on the riverbank side of the pylon (stage-11, $f = 0.346$ Hz). The modelling concept is illustrated in Fig. 5. The vertical vibration of the cantilever at the sensor position was determined by using modal analysis. By considering the first relevant bending mode, scalar equation Eq. (1) was solved by using the Newmark-beta time advancement scheme for the unknown modal displacement y_1.

$$\ddot{y}_1(t) + \gamma\omega_{01}\dot{y}_1(t) + \omega_{01}^2 y_1(t) = f_1(t) \tag{1}$$

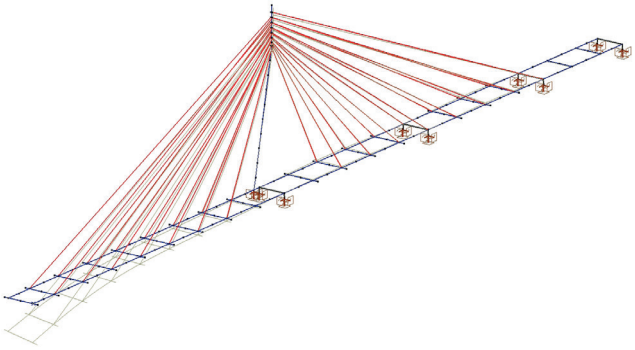

Fig. 4 Structural beam-truss model of the bridge at construction stage

The modal force on the right-hand side includes the vertical sinusoidal distributed force time function (p_y) representing the VIV forces that will be addressed later. The linear spring and viscous forces acting from the k^{th} TMD to the proper point of the deck ($Q_{TMD,k}$) were calculated from the relative displacement and velocity.

$$f_1(t) = \int \Phi_1(z) \cdot p_y(t,z)\,dz + \sum \Phi_1(z_k) \cdot Q_{TMD,k}(t) \tag{2}$$

In Eq. (1) y_1, ω_{01} and γ are the modal displacement, the circular frequency and the modal damping belonging to the first mode. In Eq. (2) $\Phi_1(z)$ is the normalized bending mode shape function, determined by the AxisVM software. The structural model was validated by a series of jumps performed by the designers at the end of the cantilever at stage-10. The TMDs were already active in this stage, but they could be inactivated by fixation. By this way, the damping of the pure steel structure as well as the effect of the TMDs could be conveniently studied. The measured and simulated vertical accelerations of the cantilever without TMDs are shown in Fig. 6. The results with TMDs can be seen in Fig. 7. The simulation time step size Δt was selected to 0.01 s based on accuracy analysis.

The jumping load (ten series of jumps) was defined to the end point of the cantilever as a periodic (piecewise-linear) discrete $P(t)$ time function instead of the distributed $p_y(t,z)$ in Eq. (1). The measured natural frequency with fixed TMDs was in the range of $f = 0.38$–0.39 Hz, slightly higher than the calculated ($f = 0.363$ Hz). The measured logarithmic decrement of damping without TMDs was close to $\delta = 0.02$, which is proposed for steel structures in Eurocode. Therefore, it was used in the further dynamic analysis as intrinsic damping of the first mode of the bridge. The measured damping with the activated TMDs was $\delta = 0.08$, which is very close to the value obtained from the simulation. To conclude, the measured and calculated

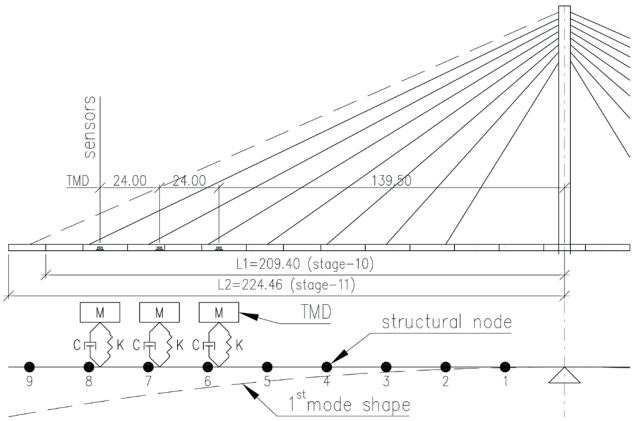

Fig. 5 Structural dynamics model of the bridge with TMD elements

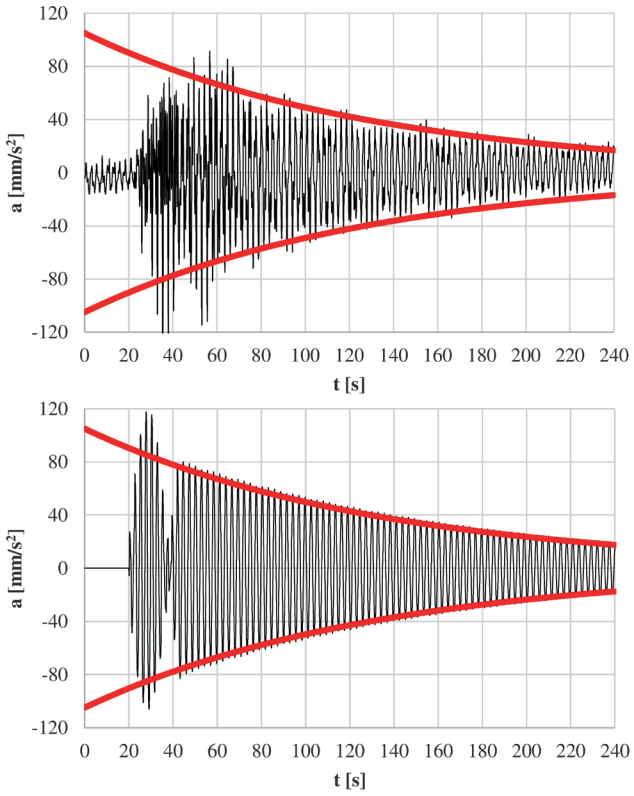

Fig. 6 Measured (top) and simulated vertical accelerations without TMDs

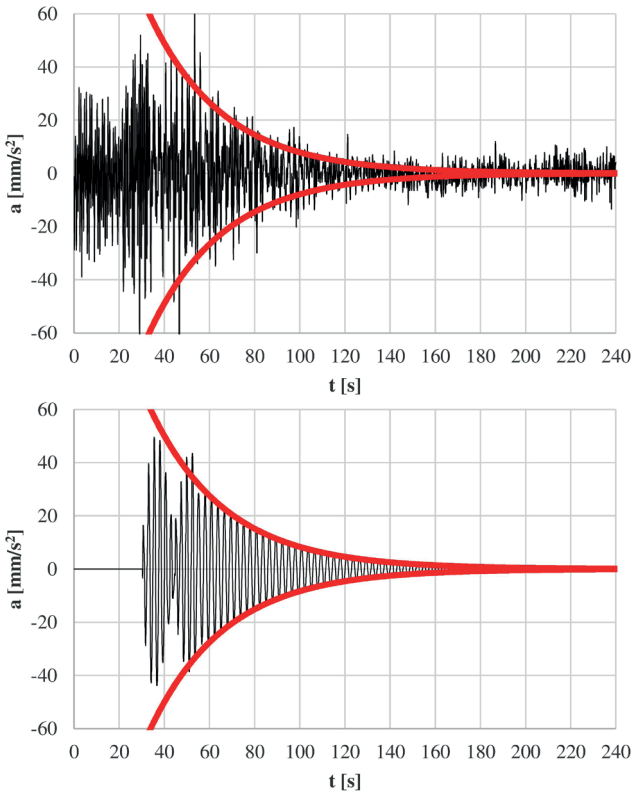

Fig. 7 Measured (top) and simulated vertical accelerations with TMDs

natural frequency and the damping values are in good agreement. The applicability of TMD during construction stages was also proved, which is practically meaningful.

4 Aerodynamics of the bridge deck

The aerodynamic parameters were simulated by utilizing open-source code OpenFOAM (version 9). The Komárom Bridge deck section was considered both at construction stage and after competition with the additional elements, such as the asphalt layer, curbs and handrails installed. The computational domain used in the two-dimensional simulations can be seen in Fig. 8. The domain sizes were determined based on recommendations found in literature in order to keep blockage ratio low.

In Reynolds-averaged models (RANS), the Navier-Stokes equation together with the continuity equation are averaged over time (denoted with overbar), resulting in averaged equations according to Eqs. (3) and (4).

$$\partial_t \overline{u}_i + \overline{u}_j \partial_j \overline{u}_i = -\frac{1}{\rho} \partial_i \overline{p} + \upsilon \partial_j \partial_j \overline{u}_i - \partial_j \overline{u_i' u_j'} \tag{3}$$

$$\partial_i \overline{u}_i = 0 \tag{4}$$

The averaging leads to new unknowns ($\overline{u_i' u_j'}$), which are referred to as the Reynolds-stresses due to velocity fluctuations. In order to close the equations, turbulence models are needed to introduce. The widely used k–ε equation turbulence model was selected due to its simplicity and low computational demand. Despite the fact, that vortex shedding problem can best be handled by the computationally more costly turbulence models, e.g., LES, k–ε model can still be used for fully developed turbulence around bluff bodies [8]. Unsteady simulations were used in accordance with the unsteady nature of the vortex shedding phenomenon.

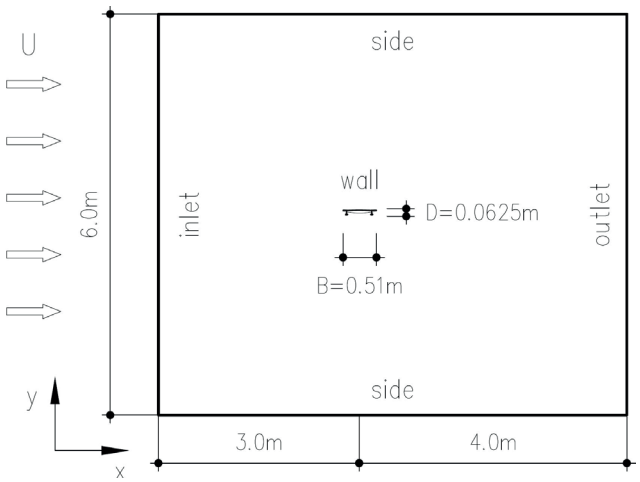

Fig. 8 The two-dimensional computational domain

The geometry size was downscaled with a scaling factor of 1:40 in order to reduce the computational efforts, which was done based on the assumption that the Reynolds number has minor effects on the aerodynamic parameters in case of an edgy bridge deck shape. At the inlet $U = 20$ m/s uniform wind velocity was defined. The turbulent kinetic energy and its dissipation rate were set uniformly according to the turbulence intensity I and the length scale L. Low ($I = 1\%$ and $L = 0.001$ m) and high ($I = 5\%$ and $L = 0.01$ m) turbulence conditions were considered in order to study its effects. The pressure gradient was set to zero. At the outlet the velocity gradient and the pressure was set to zero. On the bridge deck no slip, on the sides free slip boundary condition was defined for the wind velocity.

Besides the k–ε model, DES (Detached Eddy Simulation) model was also utilized, applied in [11, 12]. This model is the combination of RANS and LES (Large Eddy Simulation). The latter is based on filtering, instead of averaging of the Navier-Stokes equation. The filtering operation leads to the sub-grid stress tensor (SGS), which needs to be modelled. The RANS model for DES was Spallart–Allmaras (S–A), which is a one-equation model for the (modified) turbulent viscosity ($\tilde{v}_t$). The switch from RANS to LES is based on the distance from the closest wall (d) and the grid spacing (Δ) shown in Eq. (5). The DES constants of $C_{DES} = 0.65$ is offered for a wide range of applications.

$$d_{DES} = \min\left(d, c_{DES}\Delta\right) \tag{5}$$

The DES approach has a weak point of switching from RANS to LES mode too early near the wall boundary; therefore, predicts the flow separation in case of aerofoils inaccurately. In order to circumvent this problem, the length scale d_{DES} is modified considering the molecular and turbulent viscosity, leading to the delayed version of DES (DDES). At the inlet wind velocity $U = 5$ m/s, $v_t = 10^{-4}$ for turbulent viscosity were defined for low turbulence intensity ($I = 1\%$). In case of the k–ε model, coarse (mesh#1), medium (mesh#2) and fine (mesh#3) two-dimensional meshes were used. The cell numbers are approximately 25.000, 51.000 and 65.000 for the construction stage, and 38.000, 60.000 and 75.000 for the completed bridge. In case of DES the two-dimensional mesh was extruded with a length of $L = 0.60$ m and division number of $N = 60$, which is mesh#4. The total cell number for the two cross section configurations (see Fig. 9) are around 2.3 and 4.0 million, respectively. The mesh#2 around the bridge deck is shown for the completed cross section in Fig. 10.

In case of three-dimensional mesh#4 the vertical element of the handrails and curbs were replaced by longitudinal elements with equivalent drag force. The average y^+ values near the wall boundary for mesh#1, mesh#2 and mesh#3 were over 20. In case of DES, the y^+ value was kept below 1 by using properly small cells near the wall boundary and setting wind velocity U of 5 m/s, lower than in case of the k–ε model. The time step size Δt for mesh#1 was 5×10^{-5} s, for mesh#2 and mesh#3 was 2.5×10^{-5} s, for mesh#4 was 2×10^{-4} s. The velocity contour plots around the uncomplete and complete cross sections with k–ε model can be seen in Fig. 11 and Fig. 12, respectively. The simulations were performed in case of the two-cross sections, with the four meshes in both cases. Low and high turbulence intensity was considered in case of the k–ε model, and low turbulence intensity only for the DDES.

In Table 1 and Table 2 c_d, c_y' and St are the simulated static drag coefficient, the dynamic lift force coefficient (RMS of lift) and the Strouhal-number, respectively. The mesh sensitivity study of the k–ε model showed that the accuracy of mesh#2 was acceptable expect for the

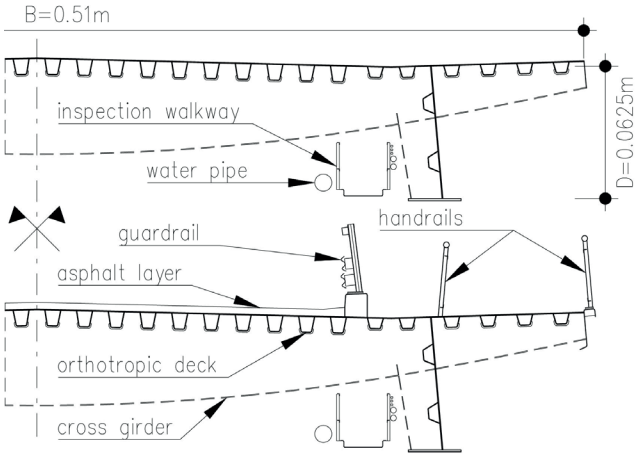

Fig. 9 Bridge deck section at construction stage and after completion

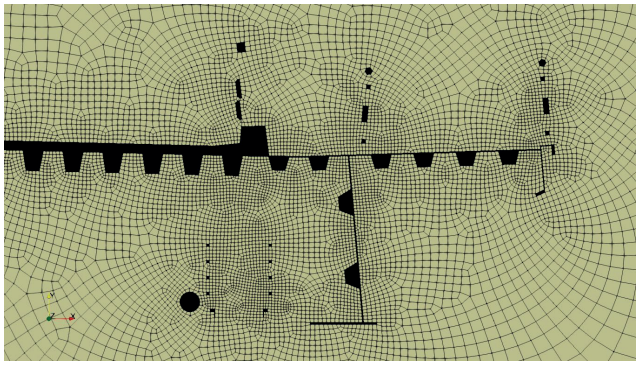

Fig. 10 Numerical mesh around the Komárom completed deck section

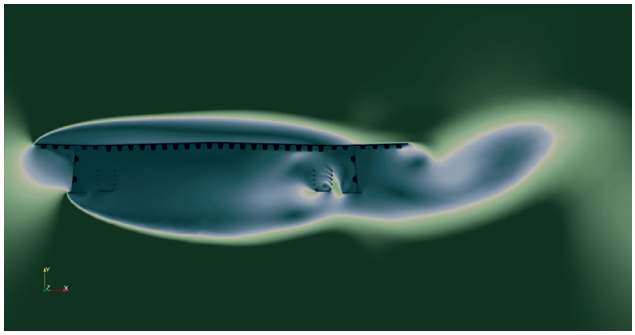

Fig. 11 Velocity contours of the deck at construction stage

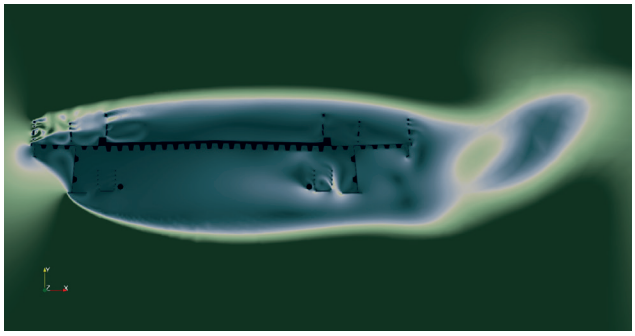

Fig. 12 Velocity contours of the completed deck

Table 1 Simulated aerodynamic parameters of the construction stage

model	I	mesh	c_D	c_y'	St
k–ε	1%	mesh#1	1.190	0.108	0.100
k–ε	1%	mesh#2	1.190	0.105	0.106
k–ε	1%	mesh#3	1.166	0.108	0.106
k–ε	5%	mesh#1	1.239	0.067	0.094
k–ε	5%	mesh#2	1.229	0.069	0.099
k–ε	**5%**	**mesh#3**	**1.236**	**0.068**	**0.100**
DDES	1%	mesh#4	1.143	0.084	0.094

Table 2 Simulated aerodynamic parameters of the final stage

model	I	mesh	c_D	c_y'	St
k–ε	1%	mesh#1	1.704	0.149	0.082
k–ε	1%	mesh#2	1.774	0.238	0.094
k–ε	1%	mesh#3	1.787	0.255	0.094
k–ε	5%	mesh#1	1.652	0.108	0.081
k–ε	5%	mesh#2	1.635	0.088	0.081
k–ε	5%	mesh#3	1.774	0.106	0.081
DDES	1%	mesh#4	1.724	0.251	0.088

completed bridge case at high turbulence. The RMS of lift coefficient showed 20 percent difference in this particular case. On the other hand, however, the convergence of drag force coefficient and Strouhal-number could be observed as a function of mesh size. The results of the k–ε and DDES models at low turbulence intensity were in reasonable agreement. Based on the results the k–ε model appeared to be appropriate to model vortex shedding phenomenon in case of the investigated specific unfavorable cross-sections. It should be mentioned, however, that it was not the case for the streamlined Humen Bridge deck section according to the Authors' study. There could be no vortex shedding observed, the flow were stabilized. The DDES model was successful only, with results of $c_y' = 0.060$ and $St = 0.095$. The detailed study is not addressed in this paper.

5 Measured wind characteristics

The monitoring system recorded wind velocities and directions as well. The wind velocity distribution within a two months deck construction period can be seen in Fig. 13. In can be seen that basically low wind speeds prevailed during the construction.

In Fig. 14 the wind direction distribution can be seen. Wind from the south-east was the most likely contrary to the north-west direction prevailing in Hungary. The bridge axis is nearly parallel with the north-south direction. The bridge cantilever was attacked under skew wind, which was unfortunate in terms of validation of simulation.

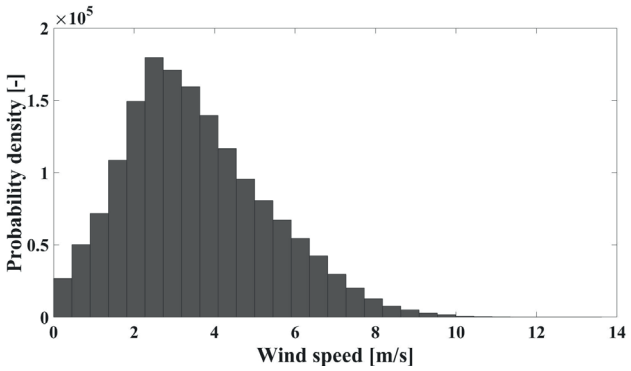

Fig. 13 Spectrum of the measured mean wind speed

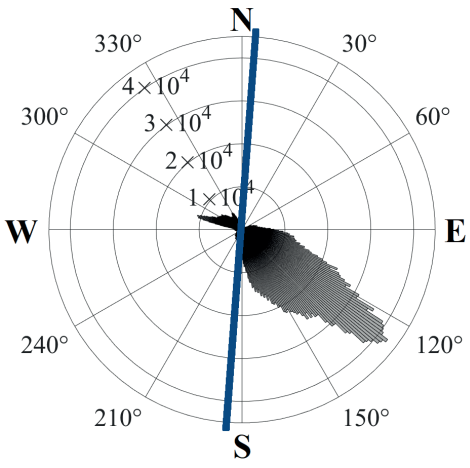

Fig. 14 Distribution of the measured wind direction

6 Validation to present monitoring data

In this section the numerical model of the Komárom Bridge was validated based on the results gained from the monitoring system dedicated to this particular structure. The relevant large amplitudes could be expected within the period of the longest cantilever stages. As was shown in Fig. 13, however, no wind velocities high enough to cause vortex induced resonance of the deck occurred; therefore, rather low vibration amplitudes could be observed only. The highest wind loading coincided with stage-11, the time series is shown in Fig. 15. The corresponding measured vertical acceleration of the TMD closest to the end of the cantilever can be seen in Fig. 16. Within approximately 20 minutes, the deck and the TMD vibration was amplified by vortex shedding of the deck as the mean wind speed grew, which is highlighted with red rectangle. The mean wind speed was around 7m/s within this time range. Other than the relevant highlighted time range, the local growth of the wind speed and that of the bridge deck acceleration coincides everywhere along the time axis, as a consequence of vortex shedding phenomenon (see Figs. 15 and 16).

The structural dynamics simulation was carried out according to model shown in Fig. 5. The dynamic load was a uniform vertical periodic excitation along the deck, except for the end of the cantilever (see Fig. 17). Due to the three-dimensional flow around the end of the deck, the excitation was assumed to be zero within a length of $4D$ = 10.5 m [13]. The mean wind speed U was 7.0 m/s, with a horizontal skewness α of 141.8° (see Fig. 14); therefore, wind speed perpendicular to the deck U was 4.33 m/s. Based on the measured frequency, lock-in was assumed, thus the excitation frequency was set to 0.346 Hz. The simulated RMS of lift (c_y' = 0.068) in case of high (5%) turbulence intensity was used, which was related to the full-scale width of the deck (B = 20.4 m). Considering the low vibration amplitudes (< 1 cm), the excitation force was constant, that is the aerodynamic forces were linear.

Within the wind speed time range marked in Fig. 15, the measured vertical acceleration of the structure and the TMD (at the position of the sensors) are shown in Fig. 18 and Fig. 19 in detail. The RMS of the acceleration of the structure and the TMD were approximately 20 mm/s^2 and 37 mm/s^2, respectively. In Fig. 20 the simulated vertical accelerations of the corresponding point of the structure and the TMD are shown.

The calculated vibration accelerations of the deck and the TMD after the transient period are 45 mm/s^2 and 95 mm/s^2, respectively (see Fig. 20), which are roughly 2.5 times higher than the corresponding measured values.

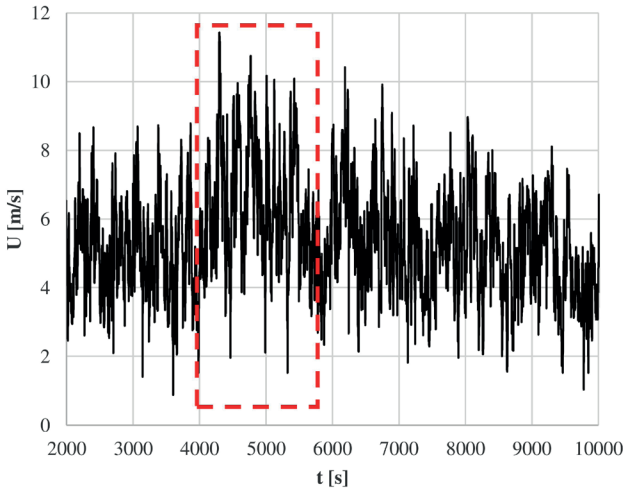

Fig. 15 Wind velocity time series

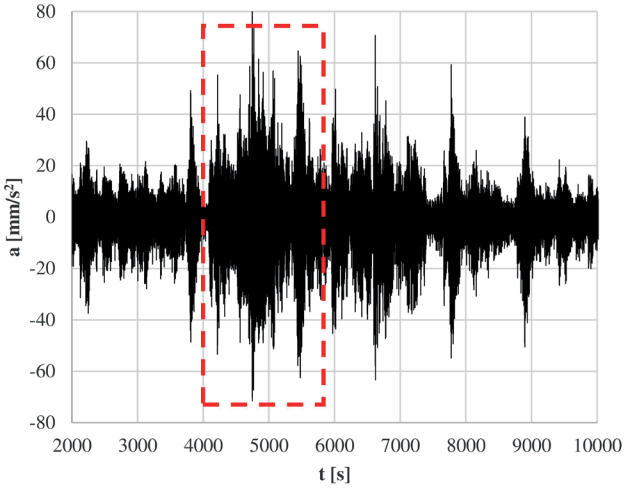

Fig. 16 Vertical acceleration time series of the TMD

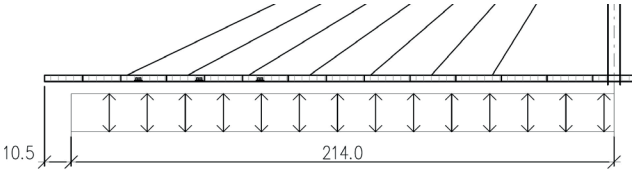

Fig. 17 VIV excitation load distribution along the cantilever

7 Conclusions

In this paper the vortex shedding excitation of the Komárom Bridge was investigated. The bridge structure was monitored during the most critical construction stages. The structural properties of the bridge were determined based on the free decay motion after a group of people excited periodically the end of the cantilever. The natural frequency of the bridge determined by the FEM model was well in line with the measurements. The measured damping of the steel structure was close to the value of steel bridges proposed by Eurocode. The damping effects of the TMD elements were also investigated by

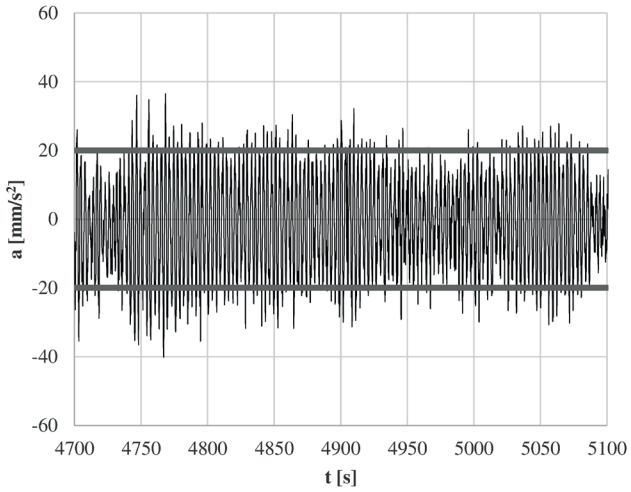

Fig. 18 Measured vertical acceleration of the structure

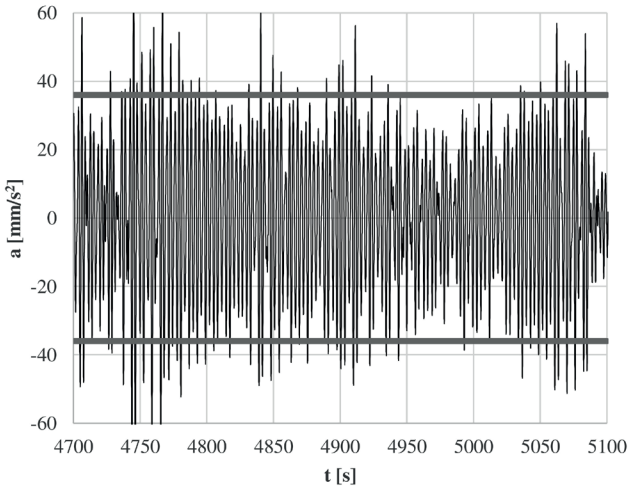

Fig. 19 Measured vertical acceleration of the TMD

the FEM model. The calculated and measured damping values were close together. The aerodynamic parameters were simulated by using CFD code. The RMS of the alternating lift coefficient and the Strouhal-number were determined by using the k-ε turbulence model. The vortex shedding phenomenon could be well captured. The simulations were performed at high and low turbulence intensities.

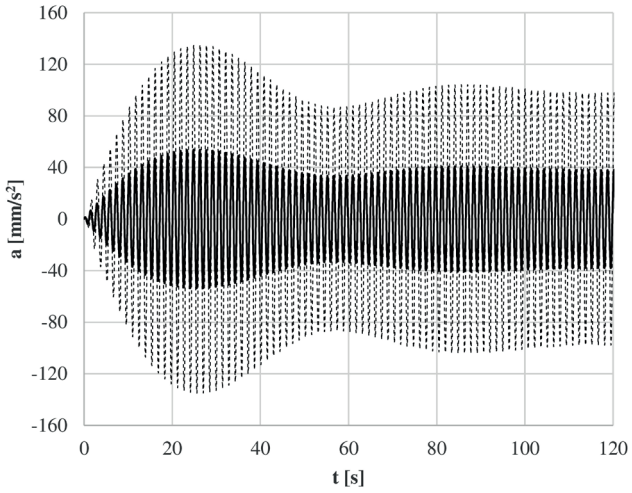

Fig. 20 Simulated acceleration of the structure (solid line) and the TMD

At low turbulence intensity, the more sophisticated DDES model was also used. The applicability of the simple k-ε model was justified based on the comparison of the results. The wind velocity magnitude and direction during the longest cantilever stage were not favorable as to study vortex induced vibrations; the cantilever with free end flow conditions and the skew wind together made simplifications necessary to make, which is assumed to be the primary reason to the rather conservative results. In order to unveil the reasons of the remarkable differences experienced in the VIV amplitudes, the three-dimensional nature of the Komárom Bridge at construction stage is planned to be studied by using full aero-elastic FSI (fluid-structure interaction) simulation that has been already utilized by the authors for flutter problems. The more sophisticated DES or LES models seem more suitable to be combined with realistic turbulent inflow conditions. Since the bridge structure is equipped with monitoring system that continuously logs wind flow and bridge deck vibration data, further detailed validation of our numerical approaches can be done in case of VIV occurrence of the completed structure.

References

[1] Zhao, L., Ge, Y. "Emergency Measures for Vortex-induced Vibration of Humen Bridge", presented at: Advances in Civil, Environmental, & Materials Research, Seoul, South Korea, Aug. 25–28, 2020.

[2] Astiz, M. A. "Wind-induced vibrations of the Alconétar Bridge, Spain", Structural Engineering International, 20(2), pp. 195–199, 2010. https://doi.org/10.2749/101686610791283696

[3] Fujino, Y., Yoshida, Y. "Wind-Induced Vibration and Control of Trans-Tokyo Bay Crossing Bridge", Journal of Structural Engineering, 128(8), pp. 1012–1025, 2002. https://doi.org/10.1061/(ASCE)0733-9445(2002)128:8(1012)

[4] CEN "EN 1991-1-4:2005, Eurocode 1: Actions on structures - Part 1-4: General actions - Wind actions", European Committee for Standardization, Brussels, Belgium, 2005.

[5] Hu, C., Zhao, L., Ge, Y. "Mechanism of suppression of vortex-induced vibrations of a streamlined closed-box girder using additional small-scale components", Journal of Wind Engineering and Industrial Aerodynamics, 189, pp. 314–331, 2019. https://doi.org/10.1016/j.jweia.2019.04.015

[6] Yang, Y., Kim, S., Hwang, Y., Kim, H.-K. "Experimental study on suppression of vortex-induced vibration of bridge deck using vertical stabilizer plates", Journal of Wind Engineering and Industrial Aerodynamics, 210, 104512, 2021.
https://doi.org/10.1016/j.jweia.2020.104512

[7] Sun, Y., Li, M., Liao, H. "Investigation on vortex-induced vibration of a suspension bridge using section and full aeroelastic wind tunnel tests", Wind and Structures, 17(6), pp. 565–587, 2013.
https://doi.org/10.12989/was.2013.17.6.565

[8] Shimada, K., Ishihara, T. "Predictability of unsteady two-dimensional k-ε model on the aerodynamic instabilities of some rectangular prisms", Journal of Fluids and Structures, 28, pp. 20–39, 2012.
https://doi.org/10.1016/j.jfluidstructs.2011.08.013

[9] Wu, T., Kareem, A. "An overview of vortex-induced vibration (VIV) of bridge decks", Frontiers of Structural and Civil Engineering, 6, pp. 335–347, 2012.
https://doi.org/10.1007/s11709-012-0179-1

[10] Huang, Z., Li, Y., Hua, X., Chen, Z., Wen, Q. "Automatic Identification of Bridge Vortex-Induced Vibration Using Random Decrement Method", Applied Sciences, 9(10), 2049, 2019.
https://doi.org/10.3390/app9102049

[11] Li, Z., Zhou, Q., Liao, H., Ma, C. "Numerical studies of the suppression of vortex-induced vibrations of twin box girders by central grids", Wind and Structure, 26(5), pp. 305–315, 2018.
https://doi.org/10.12989/was.2018.26.5.305

[12] Mannini, C. "Applicability of URANS and DES Simulations of Flow Past Rectangular Cylinders and Bridge Sections", Computation, 3(3), pp. 479–508, 2015.
https://doi.org/10.3390/computation3030479

[13] Lee, L. W., Wang, Y. L. "Aerodynamics of a circular cylinder of finite length on cross-flow", In: ASME Applied Mechanics, Bioengineering and Fluids Engineering Conference, Cincinnati, OH, USA, 1987. pp. 61–65.